Analysis of the variability in the atmospheric electric field and natural gamma radiation in different weather conditions

R. R. R. Oliveira[a*], J. Tacza[b,a], J-P. Raulin[a], S. Szpigel[a], V. Makhmutov[c], M. Philippov[c], J. G. A. Ccopa[a], A. Marun[d], G. Fernandez[e]

[a]*Center of Radio Astronomy and Astrophysics Mackenzie (CRAAM), Mackenzie Presbyterian University, São Paulo, Brazil*

[b]*Institute of Geophysics, Polish Academy of Sciences, Warsaw, Poland*

[c]*Lebedev Physical Institute, Russian Academy of Sciences, Moscow, Russia*

[d]*Instituto de Ciencias Astronómicas de la Tierra y el Espacio, San Juan, Argentina*

[e]*Complejo Astronómico El Leoncito, San Juan, Argentina*

Abstract

In recent years the analysis of the variability of the natural gamma radiation and its relationship with high atmospheric electric fields in disturbed weather, e.g., thunderstorms, have been important, as well as the relationship between these parameters in fair weather conditions. In this paper we analyze the diurnal variation of the atmospheric electric field and natural gamma radiation, in fair and disturbed weather conditions, recorded in the Argentinian Andes mountain (2552 masl) between April 2018 and February 2019. In fair weather conditions, it was found a higher linear correlation coefficient (R) between the atmospheric electric field diurnal curve and the 'universal' Carnegie curve (R=0.93), and a high negative correlation between the atmospheric electric field and natural gamma radiation diurnal curve (R=-0.9). On the other hand, in disturbed weather conditions, we reported thirteen events where it was found intense natural gamma radiation enhancements associated with high atmospheric electric field variability. A maximum of 35 % excess in the natural gamma radiation was detected, which was associated with thunderstorms and rain precipitation. It was observed a high correlation between the excesses of the gamma natural radiation enhancement with the atmospheric electric field values (R=0.80) and with the rain precipitation rate (R=0.59).

Keywords: Atmospheric Electric Field, Natural Gamma Radiation, Global Electric Circuit, lightning, Radon, Carnegie Curve

1. Introduction

The electrical nature of the atmosphere has been known since the mid-eighteenth century. Benjamin Franklin was one of the first scientists to consider phenomena such as lightning and

---

thunderstorms to be of electrical origin (Franklin, 1769). In the same century, previous studies evidenced the existence of a weak vertical atmospheric electric field (Chalmers, 1967; Beccaria, 1775). In the early twentieth century, numerous cruises around the globe performed measurements of the atmospheric electric field in fair weather conditions (absence of thunderstorms and rain precipitation) (Harrison, 2013). These measurements revealed that the atmospheric electric field in fair weather depends only on the universal time (UT), and this dependency is known as the Carnegie Curve (Mauchly, 1923). The Carnegie Curve shows values between 80 V/m and 140 V/m, with a minimum occurring at about 3 UT and a maximum at about 19 UT. The most accepted model to explain the Carnegie curve and its variability is the Global Electrical Circuit (GEC) model (Rycroft et al., 2000).

In order to explain the operating mechanism of the GEC, Wilson (1921) proposed that the planet behaves like a gigantic electrical capacitor. In this system, the Earth's surface and the ionosphere are charged plates, and the air layer between them would act like the dielectric of the system. In such models, electrical storms are the battery of the global circuit. Storm winds separate electrical charges, pulling charges from the surface and leading them to the ionosphere, generating an electric field between these two layers. Due to its high conductive, the ionosphere redistributes the charges originating from storms around the globe. In fair-weather regions, the electrical charge present in the electrosphere flows to the Earth's surface, closing the circuit (Rycroft et al., 2000). However, the GEC model does not consider the variations of the atmospheric conductivity with altitude. The variation of the atmospheric electric field vertical profile is caused by different concentrations of aerosols, variations in atmospheric density, and higher incidence of cosmic rays. This implies that the atmospheric electric field varies with altitude instead of being constant, as suggested by the GEC. To correct this inconsistency, some authors propose an Earth-Atmosphere capacitor model, where the atmospheric electric field decreases with the altitude (Haldoupis et al., 2017).

Several authors have attempted to reproduce the Carnegie Curve in fair weather conditions and its seasonal variations. In South America, Tacza et al. (2020) obtained similar variation in the local atmospheric electric field in different locations when compared with the Carnegie curve. However, differences were found associated with local effects, such as pollution, sunrise effect, and convection in the planetary boundary layer. Tacza et al. (2021) analyzed nine years of atmospheric electric measurements recorded in the Argentinian Andes and found a great correlation with the Carnegie curve, which was higher in winter than in summer. Differences in Summer were associated with convective processes in the planetary boundary layer.

In fair weather conditions, radioactive elements (mainly radon emanation) also play an essential role in modulating the atmospheric electric field. Several authors described the effect of radon on the electrical characteristics of the atmosphere. A comparison by Wilkening et al. (1966) between the positive ions generated in the decay of radon and common atmospheric ions concluded that both have similar mobility. In this way, the ions generated in the decay can affect the electrical conductivity of the atmosphere and, consequently, the atmospheric electric field. The radon concentration in the atmosphere depends primarily on meteorological conditions, e.g. temperature, humidity, rain precipitation, and wind speed. Its concentration follows a daily pattern with a maximum close to the local dawn and a minimum during the local afternoon (Barbosa, 2020). Using measurements performed in southwestern Turkey, Kulalı et al. (2016) detected seasonal variations

2

in natural gamma radiation in soil, observing higher values in winter. The authors associated this variation to high relative humidity and low temperature, meteorological conditions that support the dissolution of radon in water.

In disturbed weather conditions, thunderstorms and precipitation (rain, snow or hail) are protagonists in the modulation of the atmospheric electric field and local radioactive emission. During thunderstorms, lightning occurs due to a potential difference existing between the ground surface and electrified clouds or between the electrified clouds themselves (Srinivasan et al., 2006). According to the classification recommended by Bennett and Harrison (2007) thunderstorms have typical atmospheric electric field values above 2000 V/m. They can generate natural gamma radiation via mechanisms such as the Bremsstrahlung process and proton acceleration (Rai et al., 1972; Dwyer et al., 2012). In addition, rain precipitation causes the accumulation of radioactive particles suspended in the atmosphere close to the ground. All these processes produce an increase in natural gamma radiation near the surface (Thompson et al., 1963; Fujinami, 1996; Greenfield et al., 2003).

Investigations on the increase in natural gamma radiation after rain precipitation suggest that radon particles brought to the surface mainly come from the rain-generating cloud itself, rather than the air layer below it (Fujinami, 1996). For measurements made in Sweden, Thompson et al. (1963) observed increases in natural gamma radiation between 5 % and 20 % correlated with the occurrence of rain precipitation. The authors noted that the natural gamma radiation enhancement continued for just over 6 hours after the end of the rain precipitation. Burnett et al. (2010) found variations in the natural gamma radiation of up to 125 % above the mean values, during periods of heavy rain precipitation. These rain precipitation events were preceded by snowfalls, thus in low-temperature conditions. The gamma radiation values returned to the previous level between 1h and 2h after the end of rain precipitation. Ringuette et al. (2013), using a network of detectors located in Louisiana (USA), reported 24 natural gamma radiation enhancements associated with electrical discharges, during a period of 2.6 years. From these, only nine peaks were detected simultaneously by equipment located 1 km away, indicating a very localized effect. In addition, measurements performed in northern Israel (Reuveni et al., 2017), showed observations of natural gamma radiation enhancements after the occurrence of rain precipitation and/or electrical discharges. For events related to rain precipitation, the authors noticed a natural gamma radiation disturbance with duration up to 300 minutes. For events associated with only electrical discharges, the authors detected shorter events with duration less than 30 minutes.

In this paper, it is analyzed the atmospheric electric field and natural gamma radiation measurements recorded in the Complejo Astronomico El Leoncito, in the Argentinian Andes Mountain, in fair and disturbed weather conditions. In section 2, the instrumentation and the methods are presented. Section 3 shows the results of the atmospheric electric field and natural gamma radiation variation in different time scales during fair weather conditions (section 3.1), and during disturbed weather conditions (section 3.2). In Section 4, our results are discussed and the conclusions are presented in the final section.

2. Instrumentation and Data Analysis

In this paper, data of atmospheric electric field, natural gamma radiation, and meteorological parameters are used. The instruments are located at Complejo Astronomico El Leoncito (CASLEO) San Juan/Argentina (31° 47'S, 69° 17'W) in the Argentinian Andes Mountain. The data period is between April 2018 and February 2019. The region is characterized by an arid mountain climate, and it is located away from the nearest city, which reduces the influence of anthropogenic factors. The electric field sensor works as follows: the sensor is alternately exposed to and shielded from the external electric field. When the sensor is exposed, there is a displacement of electric charge from the ground to the sensor. When the sensor is protected from the external field, the load returns to the ground and is measured. The value of this electric current is proportional to the incident atmospheric electric field (Tacza et al., 2021). Gamma-ray data is provided by a crystal spectrometer of sodium iodide (Nal), and counts are detected by using a Hamamatsu photomultiplier tube model R1307 (Makhmutov et al., 2017). Count energy is also provided ranging between 40 keV to 5.5 meV and distributed into 128 channels. The calibration process is performed using radioactive sources Co-60 and Cs-137 . The meteorological data was obtained using a Davis model Vantage Pro2 (http://davisinstr.wpengine.com/solution/vantage-pro2/).

The first step of this study consisted of classifying the days according to the criterion of fair weather established by the United Kingdom Meteorology Office. This criterion establishes a fair-weather day when there is no precipitation (rain, snow, or hail) and wind speed is below 8m/s (Harrison, 2014). After the fair-weather days were identified, the annual and seasonal diurnal typical curves of atmospheric electric field and natural gamma radiation were calculated. The local atmospheric electric field curve and Carnegie curve were compared, and the linear correlation coefficient was calculated to verify the degree of similarity. The natural gamma radiation daily curves were correlated with the local atmospheric electric field to examine the relationship between the natural gamma radiation and the local atmospheric electric field in fair weather conditions.

In disturbed weather conditions, we selected events when there were natural gamma radiation enhancements and we analyzed its relationship with intense atmospheric electric fields and rain precipitation.

3. Results

3.1. Relationship between atmospheric electric field and natural gamma radiation in fair weather conditions

3.1.1. Classification of days according to the criterion of fair weather

Figure 1 shows the number of days classified as fair weather in each month of the analyzed period. From Figure 1, it is observed a seasonality in the distribution of the number of fair-weather days. The autumn/winter months have a larger number of fair-weather days compared to the spring/summer months. This variation was previously reported for a larger database (Tacza et al., 2021).
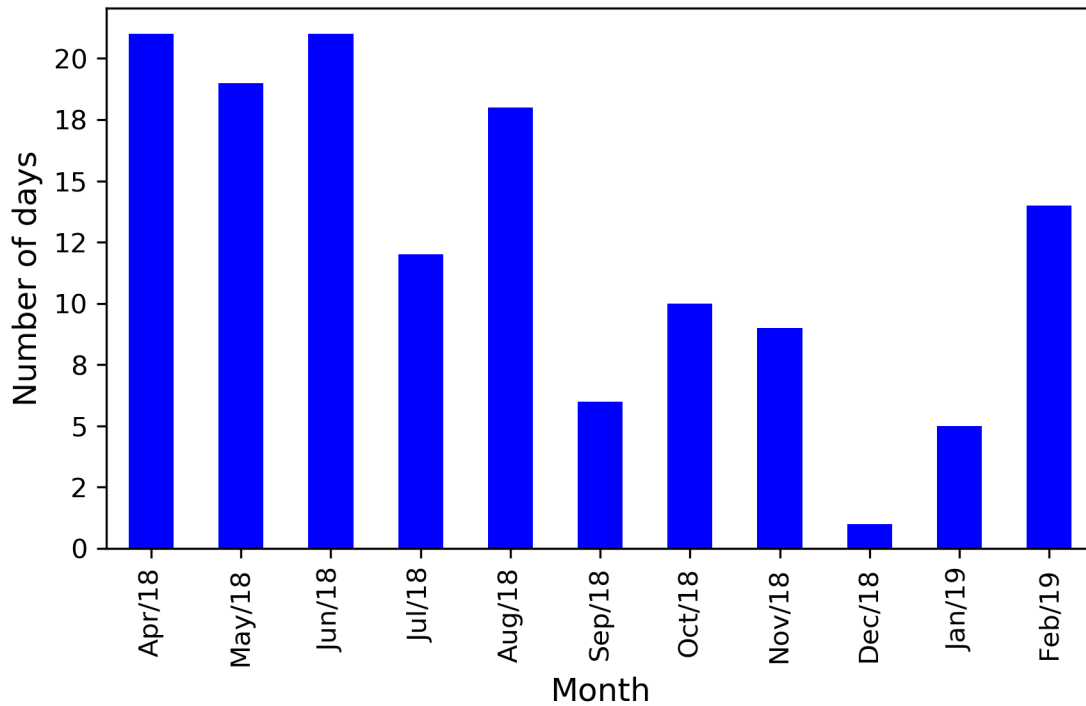
4

Figure 1: Number of fair-weather days for each month from April 2018 to February 2019.

3.1.2. Annual diurnal variation

Figure 2 shows the mean diurnal variation of absolute values (left side) and in terms of percent of the mean (right side) of the local atmospheric electric field (continuous red curve), the Carnegie curve (dashed-red curve), and natural gamma radiation (green curve).
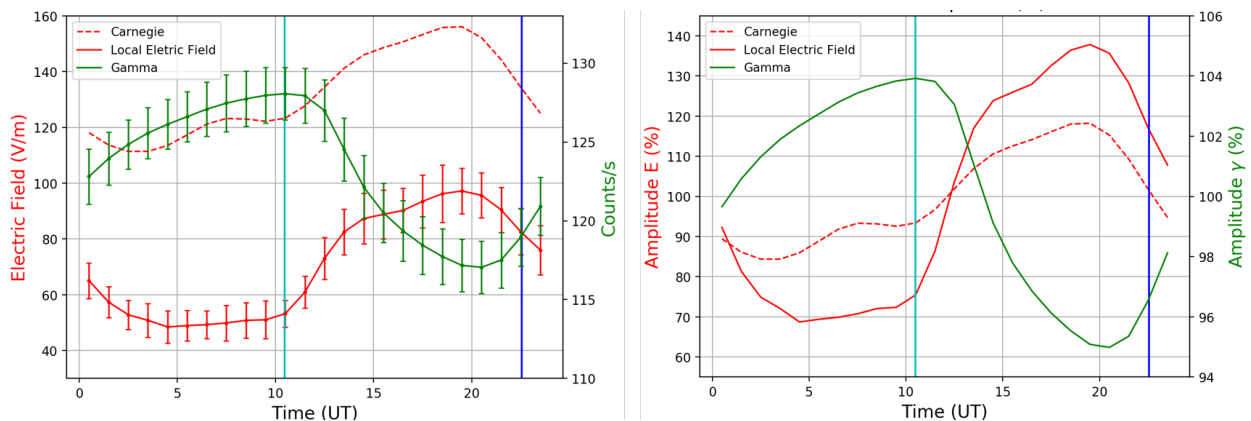

Figure 2: Mean diurnal variation of absolute values (left side) and in terms of percent of the mean (right side) of the local atmospheric electric field (continuous red curve), Carnegie curve (dashed-red curve), and natural gamma radiation (green curve) for the period from April 2018 to February 2019. The cyan and blue vertical lines indicate the sunrise and sunset times. The error bars indicate one standard deviation.

On the left side of Figure 2, we note that the local curve of the atmospheric electric field has a

5

shape similar to the Carnegie curve with a high linear correlation coefficient (R=0.93). However, the local atmospheric electric field curve shows lower absolute values by about 54 %. This could be for different reasons: site of measurement, different sensors, etc. On the right side of Figure 2, it can be observed that the local atmospheric electric field curve presents higher relative amplitude compared to the Carnegie curve. Carnegie's minimum amplitude has a value of 84.0 % between 3-4 UT (Universal Time). The local atmospheric electric field curve has a minimum amplitude of 71.7 % between 4-5 UT, that is 2 hours later than the Carnegie curve. Carnegie's maximum amplitude has a value of 118.0 %, while it is 138.8 % for the local electric field at CASLEO. Both maximum times are around 19 UT. The difference between the maximum and minimum amplitudes is 67 % and 33 % for the atmospheric electric field and for the Carnegie curve, respectively.

On the other hand, an anti-correlation between the local electric field curve and the natural gamma radiation curve is observed (R=-0.9) which could be related to both parameters responding in a different way to convective processes. This will be explained further in the next section.

Table 1 summarizes the information shown in Figure 2, i.e. the maximum and minimum times, the absolute (in V/m and counts/s) and relative (in %) values.

	Carnegie Curve	Local Atm. Field (E)	Gamma radiation (γ)
Maximum time	19 UT	19 UT	11 UT
Minimun time	3-4 UT	4-5 UT	21 UT
Maximum value	156.1 (V/m)	99.2 (V/m)	137 counts/s
Minimum value	111.4 (V/m)	51.5 (V/m)	82 counts/s
Maximum amplitude	118.0 %	138.8 %	104%
Minimum amplitude	84.0 %	71.7 %	95%
Δ amplitude	34.0 %	67.1 %	9%

Table 1: Summary of the maximum and minimum times (UT), absolute values, and relative amplitudes of the Carnegie curve, the local curve of the atmospheric electric field and natural gamma radiation.

3.1.3. Seasonal diurnal variation

Figure 3 shows the seasonal diurnal variation of the local atmospheric electric field (red curves) and natural gamma radiation (green curves) for fair weather conditions. Figures on the left side show absolute values (in V/m and counts/s) and figures on the right side show the values in terms of percent of the mean.

The seasonal atmospheric electric field diurnal curves have similar shapes in autumn, winter, and spring, with common minimum times (4-5 UT) and maximum times (19-20 UT). The exception is summer, when the maximum electric field is at 14h UT and the minimum is around 8h UT. On the other hand, the seasonal natural gamma radiation diurnal curves have similar shapes, with maximum (near local dawn at 10 UT) and minimum (20 UT) occurring at similar times for all seasons. Regarding the relative amplitude, spring and summer diurnal curves show slightly higher variation. Table 2 summarizes the information shown in Figure 3.
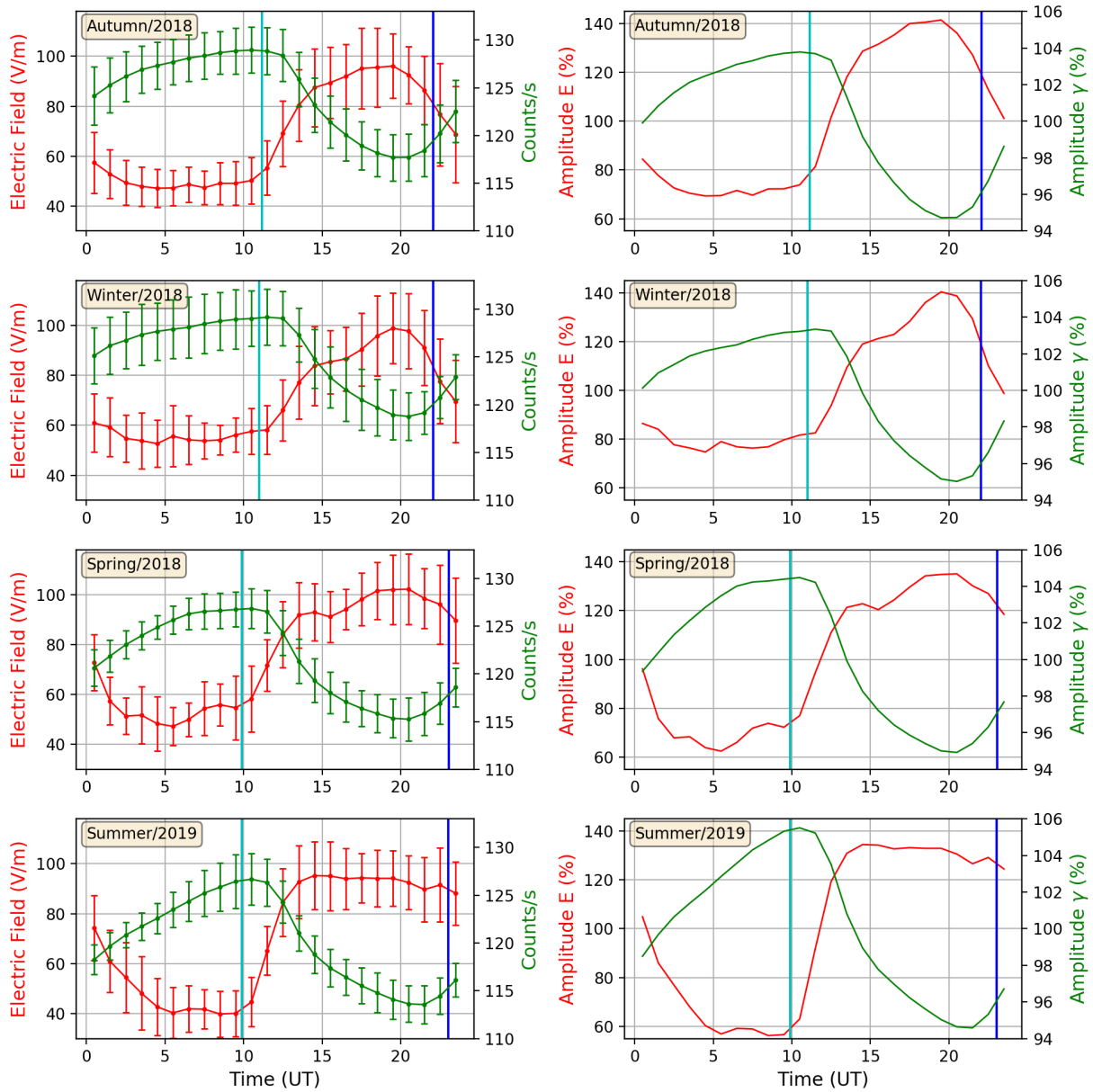
6

Figure 3: Seasonal diurnal variation of the local atmospheric electric field (red curves) and natural gamma radiation (green curves) in fair-weather days conditions, from April 2018 to February 2019. The data are expressed in absolute values (left side) and in terms of percent of the mean (right side).The cyan and blue vertical lines indicate the sunrise and sunset times. The error bars indicate one standard deviation.

	Autumn/18	Winter/18	Spring/18	Summer/18-19	Total
Max Amplitude (E)	140.4%	140.3%	135.0%	134.5%	137.8%
Min Amplitude (E)	68.8%	74.7%	62.4%	56.2%	68.7%
Amplitude(ΔE)	71.6%	65.6%	72.6%	78.3 %	69.1%
Max Time (E)	19 UT	19 UT	20 UT	14 UT	19 UT
Min Time (E)	4 UT	4 UT	5 UT	8 UT	4 UT
Max Amplitude (γ)	103.7%	103.3%	104.5%	105.5%	103.9%
Min Amplitude (γ)	94.8%	95.0%	94.9%	94.6%	95.0%
Amplitude($\Delta\gamma$)	8.9%	8.3%	9.6%	10.9 %	8.9%
Max Time (γ)	10 UT	11 UT	10 UT	10 UT	10 UT
Min Time (γ)	19 UT	20 UT	20 UT	21 UT	20 UT
R_E	0.96	0.94	0.91	0.81	0.93
R_γ	-0.90	-0.91	-0.90	-0.83	-0.89

Table 2: Maximum and minimum relative amplitudes of the atmospheric electric field and natural gamma radiation, as well as other parameters such as the difference between maximum and minimum amplitudes, the maximum and minimum times, and the linear correlation coefficients.

3.2. Relationship between atmospheric electric field and natural gamma radiation in disturbed weather conditions

A total of 13 events with natural gamma radiation enhancement were detected between April 2018 and February 2019. The excesses in the natural gamma radiation were associated with high atmospheric electric field variability and rain precipitation. Characteristics of these events such as date, duration, and excesses are listed in Table 3. Three events were associated only with thunderstorms (zero rain precipitation), and ten events were associated with thunderstorms and rain precipitation. Figures 4 and 5 show examples of these events, respectively.

Event	Start (Date / Hour UT)	Duration (minutes)	Max./ Min. E(kV/m)	E(kV/m)	% increase	Rain (mm)	Rain rate (mm/h)
1	25/01/2019 03:50 UT	260	15.4 / -2.6	18.0	16.0 %	0	0
2	27/01/2019 19:10 UT	120	5.0 / -1.0	6.0	6.0 %	0	0
3	29/01/2019 21:10 UT	370	14.1 / -11.7	25.8	15.0 %	0	0
4	03/07/2018 13:00 UT	300	2.4 / 0.2	2.6	20.0 %	1.85	1.39
5	14/10/2018 00:30 UT	220	17.5 / -10.6	28.1	21.0 %	2.95	2.95
6	14/10/2018 04:30 UT	240	5.2 / -1.1	6.3	13.2 %	3.60	1.66
7	06/01/2019 18:50 UT	300	33.9 / -30.3	64.2	35.0 %	2.25	3.38
8	14/01/2019 00:20 UT	430	25.1 / -24.5	49.6	33.0 %	2.00	2.0
9	30/01/2019 22:30 UT	360	2.4 / -23.9	26.3	13.0 %	1.25	2.50
10	01/02/2019 09:40 UT	260	8.3 / -13.7	22.0	21.0 %	1.75	1.75
11	02/02/2019 14:50 UT	310	13.3 / -15.1	28.4	23.5 %	9.00	2.57
12	02/02/2019 22:10 UT	100	1.7 / -11.0	12.7	13.8 %	2.50	1.88
13	12/02/2019 03:00 UT	720	1.4 / -21.1	22.5	10.0 %	1.75	1.50

Table 3: Events with natural gamma radiation enhancement indicating date and time of the start of the event, duration of the natural gamma radiation enhancement, the maximum and minimum values of electric field within the event, differences in absolute values between the maximum and the minimum of the atmospheric electric field, percentage of maximum increase observed in the gamma natural radiation compared with mean values, rain precipitation and rain precipitation rate.

Figure 4 shows the time profile of the atmospheric electric field (red curve) and natural gamma radiation (blue curve) diurnal curve recorded on 25 January 2019 (top panel). Dashed vertical lines identify the thunderstorm period which is shown in greater details in the middle and bottom panel. For this event, there is a sudden intense increase in the atmospheric electric field around 4 UT, reaching the maximum value of 15kV/m. At 5:30 UT, the atmospheric electric field values return to the background level. After the start of the electrical storm (at 4:20 UT), an increase in natural gamma radiation is observed. The gamma radiation values return to the background level at

8

around 7:30 UT. For this particular event the rain precipitation was zero. Figure 5 shows the event that occurred on 6 January 2019. This event presents a 35 % increase of the gamma radiation in relation to the fair-weather mean values. In general, the most natural gamma enhancements were associated with thunderstorms and rain precipitation occurring at the same time (see Table 3).
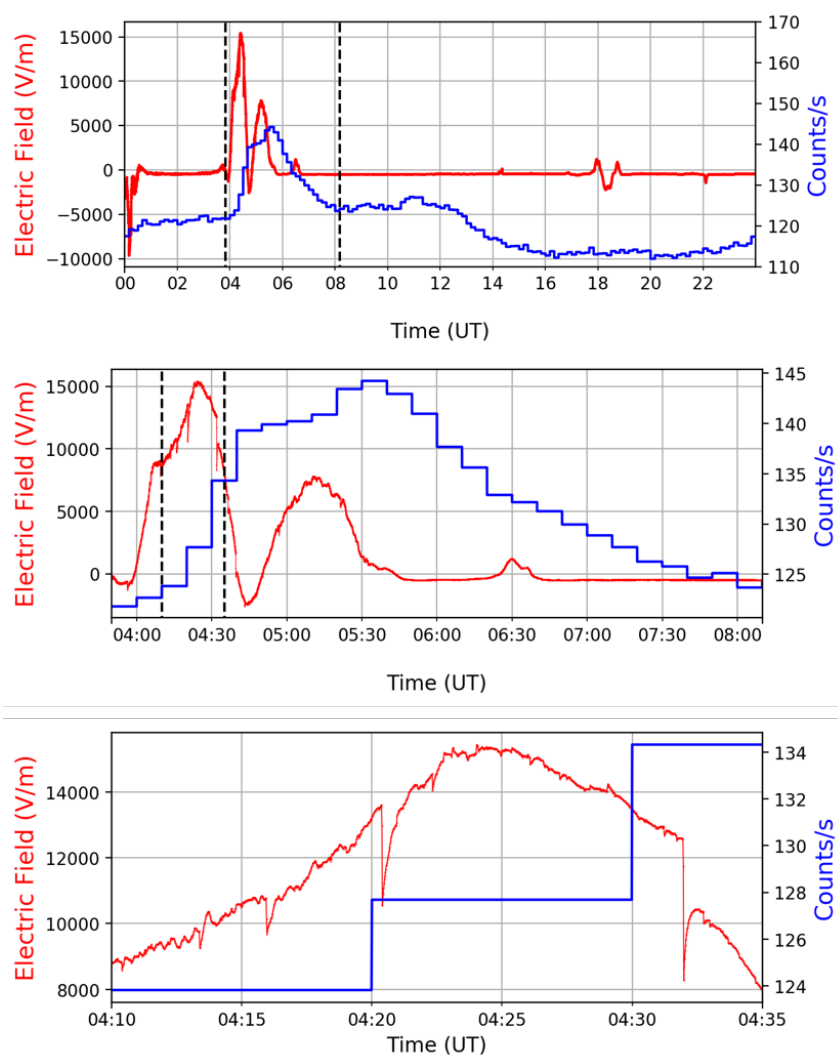

Figure 4: The local atmospheric electric field (V/m - red curve) and natural gamma radiation (counts/s - blue curve) for January 25, 2019. The figure in the top panel shows the diurnal variation for the day of the event. The middle and bottom panels show in greater detail the range of increase in the atmospheric electric field and natural gamma radiation.

Figure 5 shows the event that occurred on 6 January 2019. This event presents a 35% increase of the gamma radiation in relation to the fair-weather mean values. In general, the events with thunderstorms and rain precipitation record a high increase in natural gamma radiation (see Table 3). The event in Figure 5 shows that there is an increment in the natural gamma radiation enhancement the two phenomena are present (high electric fields and rain precipitation).
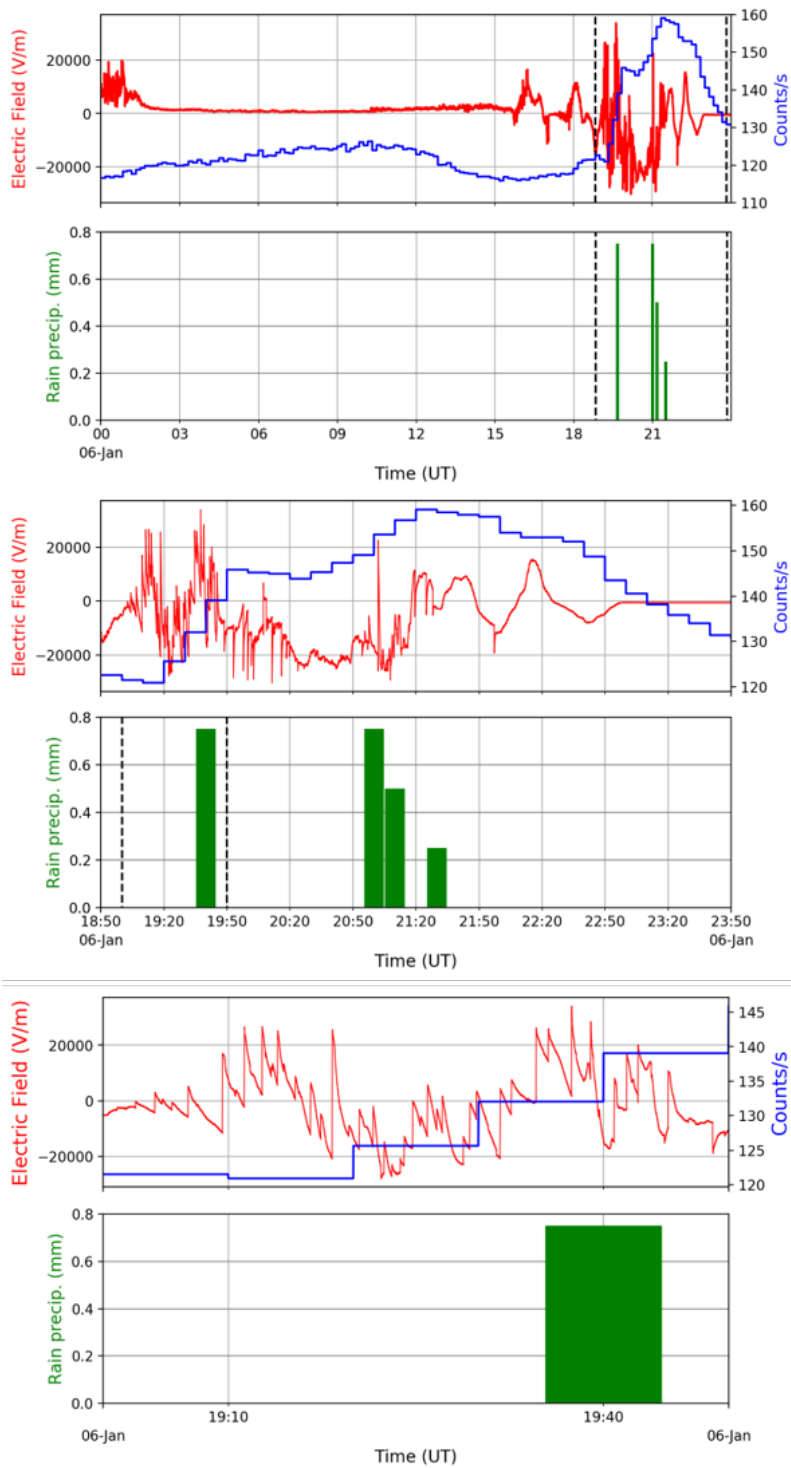
9

Figure 5: The local atmospheric electric field (V/m - red curve), natural gamma radiation (counts/s - blue curve) and rain precipitation (mm - green bars) for January 06, 2019. The figure in the top panel shows the diurnal variation for the day of the event. The middle and bottom panels show in greater detail the range of increase in the atmospheric electric field, natural gamma radiation and rain precipitation.

10

4. Discussion

4.1. Fair weather conditions

Fair weather conditions are favorable at CASLEO (as previously reported by Tacza et al. (2021). From Figure 1 it is observed a seasonality in the number of fair-weather days. The autumn/winter seasons had a greater number of fair-weather days compared with spring/summer seasons. Such differences can be explained by the higher incidence of thunderstorms and rain precipitation in the summer and spring, reducing the number of fair-weather days. On the other hand, the autumn and winter months are dry and less cloudy in favor of fair-weather conditions.

The great similarity between the local atmospheric electric field diurnal curve and the 'universal' Carnegie curve was previously reported (Tacza et al., 2014, 2021). However, two main differences are evidenced (Figure 2): the difference in the absolute values and the difference in the relative amplitude values. These differences can be explained by the action of ionizing agents. The Carnegie curve was measured above the ocean, which reduces the local effects drastically, and the atmospheric electric field diurnal curve at CASLEO is influenced by local effects (such as radioactive elements, pollution, and humidity) which change the atmospheric electrical conductivity and, therefore, modify the local atmospheric electric field (Tacza et al., 2021). On the other hand, it is also observed from Figure 2 that the natural gamma radiation diurnal curve had a typical daily variation. The maximum natural gamma radiation occurs at the local dawn (~10UT), with little turbulent atmospheric conditions, and the minimum occurs at the local afternoon (~20UT), with maximum peak in the atmospheric turbulence.

From Figure 3, it was observed higher absolute values in the natural gamma radiation curve in autumn/winter seasons; however, the spring/summer diurnal curves show greater relative amplitude. These seasonal differences can be explained by the action of convective forces (such as wind speed and temperature), as they scatter the suspended radioactive elements and are more intense in the spring and summer. Furthermore, as mentioned in the introduction part, the main radioactive component suspended in the atmosphere is radon, and one of its properties is its solubility inversely proportional to the temperature. Therefore, low temperatures and more stable weather conditions facilitate the accumulation of radon and increase the amplitude of the natural gamma radiation curve. These conditions are most certainly found in autumn and winter and may explain the seasonal variation.

On the other hand, from Figure 3 it is observed that the atmospheric electric field diurnal curves have similar shapes in autumn, winter, and spring. Maximum and minimum peaks occur at similar times. The exception is summer, when the maximum atmospheric electric field is at 14 UT, and the minimum is around 8 UT. This is due to more convective processes occurring in summer that influence the electric field. This was explained in detail in Tacza et al. (2021).

In summary, for fair weather conditions we observed that natural gamma radiation and the atmospheric electric field diurnal curves react in a different way. At night, in stable conditions, there is a high accumulation of radon which generates an increase in the natural gamma radiation. After sunrise, the temperature increases, which produces convection and turbulence, dissipating the radon concentration (and therefore we observe a decrease in gamma radiation), and increasing the atmospheric electric field.

11

4.2. Disturbed weather conditions

Table 3 indicates the natural gamma radiation enhancement events and the main features of the atmospheric electric field and rain precipitation that were associated with these events. Ten events were associated with the occurrence of thunderstorms and rain precipitation (see one of them in Figure 5) and three events were associated only with thunderstorms (with zero rain precipitation, see one of them in Figure 4). The excesses observed ranged from 5 % to 35 % and had a duration between 50 and 590 minutes. The results indicate that the natural gamma radiation enhancements are related to the processes of electrical discharges (lightning) and rain precipitation. As described by Greenfield et al. (2003) and Ringuette et al. (2013), thunderstorms are sources of gamma radiation enhancement generated by the Bremsstrahlung process; therefore, our observations may be related with this process. Natural gamma radiation enhancement can also be associated with rain precipitation, as the precipitation causes the effect of accumulation of radioactive material suspended in the atmosphere close to the Earth's surface Greenfield et al. (2003) and Ringuette et al. (2013). For the analyzed period, it was not observed a natural gamma enhancement only associated with rain precipitation, i.e., without the occurrence of thunderstorms. From Table 4 it is noted that the events in which there is a greater natural gamma radiation enhancement were associated with thunderstorms and rain precipitation occurring together. We speculated that there is a superposition of the natural gamma radiation enhancement produced by the Bremsstrahlung processes (occuring in thunderstorms) and by the radioactive material accumulation on the Earth's surface (brought by rain precipitation). These results are in agreement with previous reports (e.g., Burnett et al. (2010); Reuveni et al. (2017)).

In Figure 6 is shown the linear relationship between the natural gamma radiation enhancement with the intensity of the atmospheric electric field (top panel) and with the rain precipitation rate (bottom panel). The Pearson linear correlation coefficients are R_E=0.80 (atmospheric electric field) and R_r = 0.59 (rain precipitation), respectively. Further studies are necessary to evaluate the correct contribution of each parameter (atmospheric electric field and rain precipitation) in the natural gamma radiation enhancement.

5. Conclusion

In this paper, we analyzed the variations in the atmospheric electric field and natural gamma radiation in different weather conditions. For fair weather conditions, we found a high correlation between the atmospheric electric field mean diurnal curve with the 'universal' Carnegie curve (R=0.93). Both curves showed the same maximum time (at 19 UT) but slightly different in the minimum time. Furthermore, the relative amplitudes of the atmospheric electric field, found at CASLEO, are higher than the Carnegie curve, possibly associated with convective processes. The mean diurnal variation in the natural gamma radiation is anticorrelated with the atmospheric electric field curve (R=-0.89). In fair weather conditions, both parameters respond in a different way to convective processes. On the other hand, for disturbed weather we reported thirteen natural gamma radiation enhancements which were associated with the occurrence of thunderstorms and rain precipitation. The most significant excesses in the natural gamma radiation were associated with thunderstorms and rain precipitation occurring at the same time. The most intense excess detected in the natural gamma radiation was of 35.0 %, for the period analyzed.
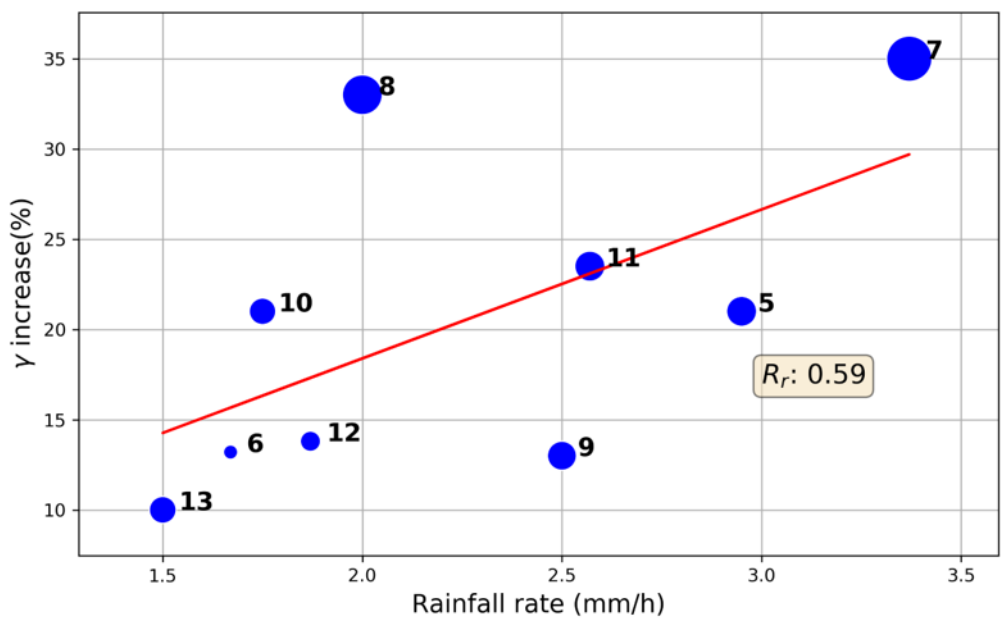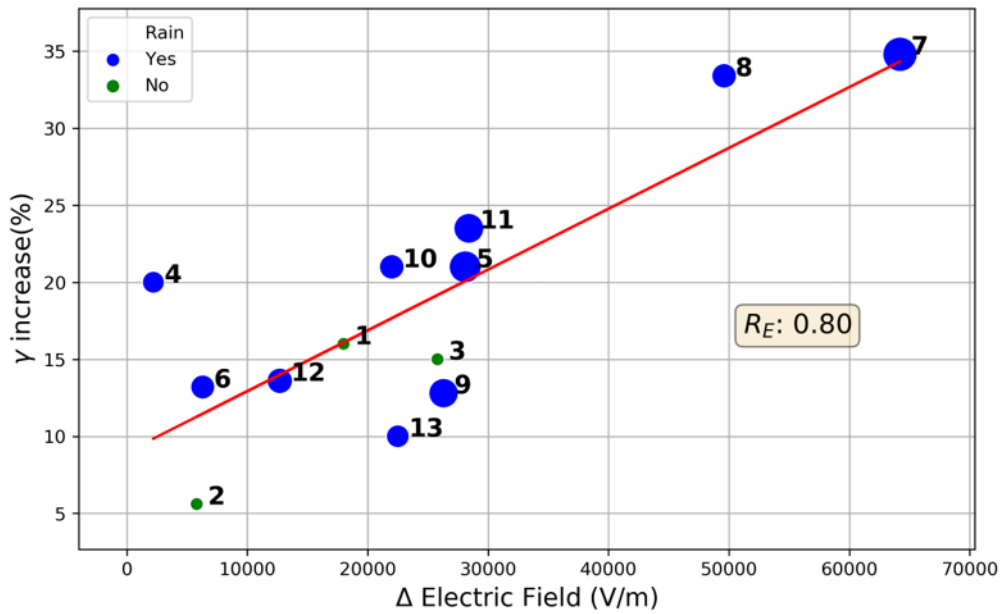
Figure 6: Top panel: Natural gamma radiation enhancements versus the intensity of the atmospheric electric field observed for each event of Table 3. Green circles represent events without rain precipitation. Blue circles represent events with rain precipitation. The size of the circle is proportional to the precipitation rate of the event. Bottom panel: Natural gamma radiation enhancements versus the rain precipitation rate (in mm/h).

6. Acknowledgments

13

References

Barbosa, S., 2020. Ambient radioactivity and atmospheric electric field: A joint study in an urban environment. Journal of Environmental Radioactivity 219, 106283.

Beccaria, G., 1775. Della elettricita terrestre atmosferica a Cielo Sereno. na.

Bennett, A., Harrison, R., 2007. Atmospheric electricity in different weather conditions. Weather 62, 277–283.

Burnett, J., et al., 2010. Short-lived variations in the background gamma-radiation dose. Journal of Radiological Protection 30, 525.

Chalmers, J., 1967. Atmospheric electricity pergamon press. New York , 128.

Dwyer, J., et al., 2012. High-energy atmospheric physics: Terrestrial gamma-ray flashes and related phenomena. Space Science Reviews 173, 133–196.

Franklin, B., 1769. Experiments and observations on electricity, made at Philadelphia in America... To which are added, letters and papers on philosophical subjects. The whole corrected, methodized... and now first collected into one volume, etc.[Edited by Peter Collinson.]. David Henry.

Fujinami, N., 1996. Observational study of the scavenging of radon daughters by precipitation from the atmosphere. Environment International 22, 181–185.

Greenfield, M., et al., 2003. Near-ground detection of atmospheric γ rays associated with lightning. Journal of applied physics 93, 1839–1844.

Haldoupis, C., et al., 2017. Is the "earth-ionosphere capacitor" a valid component in the atmospheric global electric circuit? Journal of Atmospheric and Solar-Terrestrial Physics 164, 127–131.

Harrison, R.G., 2013. The carnegie curve. Surveys in Geophysics 34, 209–232.

Harrison, R.G., 2014. Fair weather atmospheric electricity: its origin and applications, in: Proc. ESA Annual Meeting on Electrostatics, p. 1.

Kulalı, F., et al., 2016. Investigation of the radon levels in groundwater and thermal springs of pamukkale region. Acta Physica Polonica A 130, 496–498.

Makhmutov, V., Stozhkov, Y., Raulin, J.P., Philippov, M., Bazilevskaya, G., Kvashnin, A., Tacza, J., Marun, A., Fernandez, G., Viktorov, S., et al., 2017. Variations in cosmic rays and the surface electric field in january 2016. Bulletin of the Russian Academy of Sciences: Physics 81, 241–244.

Mauchly, S., 1923. On the diurnal variation of the potential gradient of atmospheric electricity. Terrestrial Magnetism and Atmospheric Electricity 28, 61–81.

Rai, J., et al., 1972. Bremsstrählung as a Possible Source of UHF Emissions from Lightning. Nature Physical Science 238, 59–60. doi:10.1038/physci238059a0.

Reuveni, Y., et al., 2017. Ground level gamma-ray and electric field enhancements during disturbed weather: Combined signatures from convective clouds, lightning and rain. Atmospheric research 196, 142–150.

Ringuette, R., et al., 2013. Tetra observation of gamma-rays at ground level associated with nearby thunderstorms. Journal of Geophysical Research: Space Physics 118, 7841–7849.

Rycroft, M., et al., 2000. The global atmospheric electric circuit, solar activity and climate change. Journal of Atmospheric and Solar-Terrestrial Physics 62, 1563–1576.

Srinivasan, K., et al., 2006. Lightning as atmospheric electricity, in: 2006 Canadian Conference on Electrical and Computer Engineering, IEEE. pp. 2258–2261.

Tacza, J., Raulin, J.P., Macotela, E., Norabuena, E., Fernandez, G., Correia, E., Rycroft, M., Harrison, R., 2014. A new south american network to study the atmospheric electric field and its variations related to geophysical phenomena. Journal of Atmospheric and Solar-Terrestrial Physics 120, 70–79.

Tacza, J., Raulin, J.P., Morales, C., Macotela, E., Marun, A., Fernandez, G., 2021. Analysis of long-term potential gradient variations measured in the argentinian andes. Atmospheric Research 248, 105200. URL: http://www.sciencedirect.com/science/article/pii/S0169809520311364, doi:https://doi.org/10.1016/j.atmosres.2020.105200.

Tacza, J., et al., 2020. Local and global effects on the diurnal variation of the atmospheric electric field in south america by comparison with the carnegie curve. Atmospheric Research 240, 104938. URL: http://

www.sciencedirect.com/science/article/pii/S0169809519313237, doi:https://doi.org/10.1016/j.atmosres.2020.104938.

Thompson, T., et al., 1963. Some observations of variations of the natural background radiation. Tellus 15, 313–318.

Wilkening, M., et al., 1966. Radon-daughter ions and their relation to some electrical properties of the atmosphere. Tellus 18, 679–684.

Wilson, C.T.R., 1921. Iii. investigations on lighting discharges and on the electric field of thunderstorms. Philosophical Transactions of the Royal Society of London. Series A, Containing Papers of a Mathematical or Physical Character 221, 73–115.